

A current cycle feedback iterative learning control approach to AFM imaging[‡]

Ying Wu* and Qingze Zou[†]

Mechanical Engineering Department, Iowa State University
Ames, IA, 50011

* wuying@iastate.edu; [†] qzzou@iastate.edu

Chanmin Su[§]

Veeco Instruments Inc.
Santa Barbara, CA, 93117

[§] CSu@veeco.com

Abstract—In this article, we proposed a novel current cycle feedback (CCF) iterative learning control (ILC) approach to achieve high-speed imaging on atomic force microscope (AFM). AFM-imaging requires precision positioning of the AFM probe relative to the sample in 3-D (x - y - z) dimension. It has been demonstrated that with advanced control techniques such as the inversion-based iterative-control (IIC) technique, precision positioning of the AFM probe in the lateral (x - y) direction can be successfully achieved. Additional challenges, however, must be overcome to achieve precision positioning of the AFM-probe in the vertical direction. The main contribution of this article is the development of the CCF-ILC approach to the AFM z -axis control. Particularly, the proposed CCF-ILC controller design utilizes the recently-developed robust-inversion technique to minimize the model uncertainty effect on the feedforward control, and remove the causality constraints existing in other CCF-ILC approaches. Experimental results for AFM imaging are presented and discussed to illustrate the proposed method.

I. INTRODUCTION

In this article, we propose a current circle feedback (CCF) iterative learning control (ILC) approach for tracking the unknown sample topography during AFM imaging. The nanoscale resolution of the AFM has made the AFM an enabling tool to image as well as manipulate matters at the nanoscale [1]. Current AFM system, however, is slow and thereby AFM imaging is time consuming. Such slow speed of AFM has hindered the use of AFM to interrogate nanoscale dynamic phenomena. AFM imaging demands the precision positioning of the AFM probe relative to the sample in all x , y , z -axes 3-D dimension. It has been demonstrated that with advanced control techniques [2] such as the inversion-based iterative control (ILC) [2], precision positioning of the AFM probe at high speed can be successfully achieved in the lateral (x , y -axes) direction. Challenges, however, must be overcome to achieve the precision positioning of the AFM-probe in the vertical z -axis, because 1) the sample topography is unknown in general, 2) the probe-sample interaction is complicated due to the nonlinear dependence of the interaction force on the probe-sample position as well as the deformation/reaction of the sample [3], [4], and 3) the relative probe-sample position is sensitive to the probe-sample interaction [4]. Therefore, there exists need to improve the z -axis AFM controller design to achieve high-speed AFM imaging.

[‡]The work is supported by the NSF Grants CMS-0626417 and DUE-0632908.

Various control approaches have been developed for the z -axis precision positioning of the probe during the AFM imaging. For example, PI-type of controllers have been widely used in commercial AFM systems. Such ad-hoc controllers, however, have severe bandwidth limitation and poor robustness, because of the low gain margin of the piezo actuators. Modern model-based feedback control approach increases the system bandwidth and achieves better robustness [5]. However, the bandwidth and robustness of these feedback-based approaches are still limited by the fundamental limitations of closed-loop system — the performance of all feedback control systems is governed by the well-known Bode's integral. Thus, in these advanced feedback control approaches, large bandwidth has to be traded off with the system robustness. Moreover, the performance of feedback control is further limited for the nonminimum-phase systems. These constraints of feedback approaches to the z -axis control of AFM imaging, can be alleviated by combining the feedback control with the feedforward control. For example, in the two-degree-of-freedom (2DOF) design approach presented in [5], the feedback and the feedforward controllers were designed based on the H_∞ robust control theory. Although the AFM imaging speed can be increased, limits still exist in such a 2DOF controller design. First, the H_∞ -based feedforward controller is causal (i.e., stable), therefore, as piezo actuators tend to be minimum-phase, the performance of such feedforward controller can be limited. Moreover, the "bandwidth" of the feedforward control is restricted by the bandwidth of the feedback control, because the current feedforward control signal is generated by using the total control signal for the last scanline. Therefore, there exists a need to better design the 2DOF control approach by overcoming the causality and bandwidth limitations in the z -axis control in the AFM imaging.

The main contribution of this article is the development of a novel CCF-ILC approach to achieve z -axis precision positioning during the AFM imaging. Particularly, we decouple the bandwidth requirement from the robustness requirement in the proposed 2DOF control approach: the feedback controller is designed mainly to enhance the robustness of the entire system, and the feedforward control is designed to enlarge the bandwidth by overcoming the minimum-phase constraint of the piezo dynamics, and utilizing the noncausality through iterations to improve the tracking. Specifically, the feedback controller is designed based on the H_∞ robust

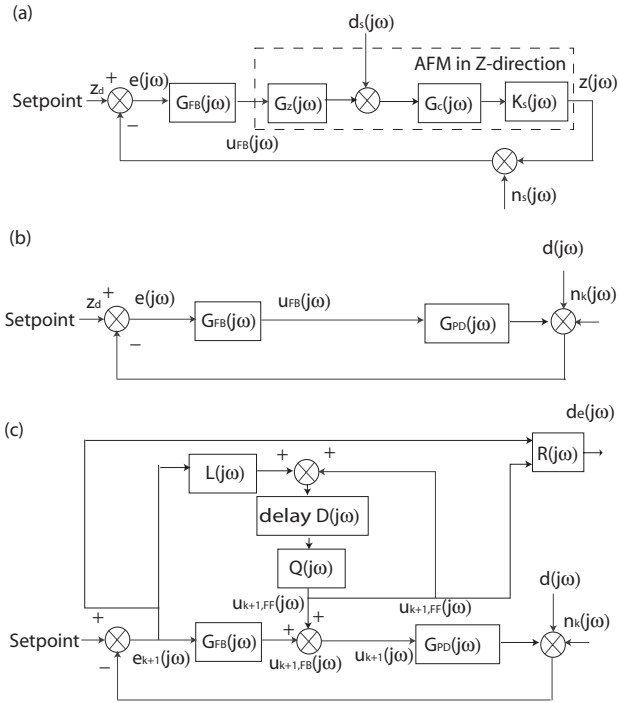


Fig. 1. The block diagram of (a) a standard feedback loop, (b) the modified feedback loop, and (c) the proposed CCF-ILC approach for the z -axis positioning in AFM imaging.

control theory [6], and the robust-inverse [7] is introduced into the ILC filter design to explicitly account for the dynamics uncertainty in the feedforward control. The proposed CCF-ILC control approach is illustrated by implementing it to the z -axis direction control in AFM imaging. Experimental results show that the imaging speed can be significantly increased by using the proposed approach.

II. PROBLEM FORMULATION AND ANALYSIS

In this section, we present the inversion-based CCF-ILC approach to the vertical z -axis positioning of the AFM probe during imaging. The key feature of the proposed approach is that the feedforward control input is updated online (through iterations) and applied, which is augmented to the z -axis feedback control (see Fig. 1(c)). We start with briefly describing the z -axis feedback control.

The feedback control system for z -axis AFM probe positioning is shown in Fig. 1(a), where $G_z(s)$ denotes the dynamics model of the piezo actuator for the z -axis positioning, $G_c(s)$ denotes the dynamics from z -axis piezo output to the cantilever deflection (including the cantilever and the mechanical linkage from the piezo actuator to the cantilever), and $K_s(s)$ denotes the photodiode sensitivity. The goal of the z -axis AFM probe positioning is to maintain a constant setpoint value (i.e., constant normal force between the tip and the sample) during the scanning process. Then the image of the sample topography can be estimated using the control signal or the deflection error [8].

We note that the bandwidth of the cantilever and the photodiode dynamics tends to be much higher (over 10 times) than that of the z -axis piezo dynamics. Therefore, the sample profile in the z -axis feedback control loop shown in Fig. 1 (a)

can be scaled by the DC-Gain of the cantilever-photodiode dynamics, and then shifted right to close to the cantilever deflection output, as in the block diagram in Fig. 1 (b). This signal shifting is utilized in the proposed CCF-ILC approach to simplify the presentation.

The proposed CCF-ILC design is shown in Fig. 1 (c). Particularly, the objectives of the controller design are to:

- 1) Guarantee the convergence of the CCF-ILC approach, i.e., the feedforward control input $u_{k,FF}(j\omega)$ remains bounded during all iterations k , and the residual error $e_k(j\omega)$ converges to zero when the noise $n(j\omega)$ vanishes;
- 2) Improve the feedback tracking with the augmented feedforward control, i.e., for the same feedback controller, the tracking error $e(j\omega)$ (e.g., the deflection signal) is smaller when using the CCF-ILC approach than that when using the feedback control alone;
- 3) Improve the imaging accuracy, i.e., the estimation of the sample profile $d_s(j\omega)$ is more accurate than that obtained by using current commercial AFMs.

We note that the proposed CCF-ILC approach aims at achieving high-speed imaging of samples with relatively smooth topography. For these samples, the sample profile of two adjacent scanlines are similar, and thereby such a similarity can be exploited to improve imaging speed. As the first step, this article focuses on the precision tracking of the sample profile on one scanline.

In the proposed CCF-ILC technique, feedback controller is designed first. It is noted that it is desirable that the feedback controller should be robust against model uncertainties and noise effects. Thus, the feedback controller is designed to enhance the robustness of the entire control system. We design the feedback controller by using the robust control technique [6] (The readers are referred to [7] for details).

A. CCF-ILC Algorithm: Convergence Analysis

In the proposed CCF-ILC approach, the following general form of linear iterative learning control law is employed [9]:

$$u_{0,FF}(j\omega) = 0$$

$$u_{k+1,FF}(j\omega) = Q(j\omega)(u_{k,FF}(j\omega) + L(j\omega)e_k(j\omega)), \quad (1)$$

for $k \geq 1$

where $Q(j\omega)$ and $L(j\omega)$ are the ILC filters to be designed. Note that in Eq. (1), the filter $Q(j\omega)$ is factored out without loss of generality. The conditions to guarantee the convergence of the CCF-ILC algorithm (the first objective) is given by the following lemma.

Lemma 1: Let $G_{PD}(j\omega)$ be the frequency response of a linear time invariant plant, and let $G_{FB}(j\omega)$ be a stabilizing feedback controller. Then for bounded measurement noise $n_k(j\omega)$, i.e., $|n_k(j\omega)| \leq \delta(\omega)$, in the CCF-ILC algorithm (1) (see Fig. 1 (c)), the iterative control input $u_k(j\omega)$ is bounded all the time and the residue error $e_k(j\omega)$ converges to zero with small remaining error (which is called as ‘ultimate ILC error’ in the following), where the ultimate ILC error $e_\infty(j\omega)$ is an affine function of the sample profile $d(j\omega)$ and

the noise effect $\delta(\omega)$.

$$\begin{aligned} |e_\infty(j\omega)| &\triangleq \lim_{k \rightarrow \infty} |e_k(j\omega)| \\ &\leq \left| \frac{r(\omega)}{1 - \rho(\omega)} \right| |d(j\omega)| + E_\delta(j\omega)\delta(\omega) \end{aligned} \quad (2)$$

provided that the ILC filters $L(j\omega)$ and $Q(j\omega)$ are chosen to render the following iteration coefficient $\rho(j\omega)$ to be less than one, i.e.,

$$\rho(\omega) = |Q(j\omega) \{1 - G_{PD}(j\omega)S(j\omega)L(j\omega)\}| < 1. \quad (3)$$

In Eq. (2), the frequency dependent variable $r(\omega)$ and $E_\delta(j\omega)$ is defined as

$$r(\omega) \triangleq |(Q(j\omega) - 1)S(j\omega)| \quad (4)$$

$$E_\delta(\omega) \triangleq \frac{|Q(j\omega)G_{PD}(j\omega)S(j\omega)L(j\omega)S(j\omega)| + |S(j\omega)|}{|1 - \rho(\omega)|}$$

III. DESIGN OF THE ILC FILTERS

Next we discuss the design of the ILC filters, $Q(j\omega)$ and $L(j\omega)$. In the following, $Q(j\omega)$ is named as the ‘roll-off ILC filter’ and $L(j\omega)$ as the ‘inversion-based ILC filter’. We propose a two-step approach to design the ILC filters $Q(j\omega)$ and $L(j\omega)$. Note that Lemma 1 shows that the ultimate error coefficient $r(\omega)$ (as defined in Eq. (4)) is independent to the design of the inversion-based ILC filter $L(j\omega)$. Thus, we first design the inversion-based ILC filter $L(j\omega)$ — based on the recently-developed robust-inversion technique [7] — to minimize the iteration coefficient $\rho(\omega)$, i.e., find $L(j\omega)$ such that the term $|1 - G_{PD}(j\omega)S(j\omega)L(j\omega)|$ is minimized upon system dynamics uncertainties. Then secondly, the roll-off ILC filter $Q(j\omega)$ is designed to ensure the convergence of the CCF-ILC algorithm, and to minimize the ultimate error $e_\infty(j\omega)$ (see Eq. (2))

A. Design of the inversion-based ILC filter $L(j\omega)$

The design objective of the ILC filter $L(j\omega)$ is to minimize the feedforward control error $|1 - G_{PD}(j\omega)S(j\omega)L(j\omega)|$ while accounting for the system dynamics uncertainties, i.e.,

$$\min_{\alpha(\omega)} \sup_{\Delta G} |1 - G_{PD}(j\omega)S(j\omega)L(j\omega)|, \quad (5)$$

where ΔG denotes the model uncertainties defined below [7], [10]:

$$\Delta G(j\omega) = \frac{G_L(j\omega)}{G_{L,m}(j\omega)} = \Delta r(\omega) \cdot e^{j\Delta\theta(\omega)}. \quad (6)$$

In Eq. (6), $G_L(j\omega)$ denotes the true linear dynamics response of the system, e.g.,

$$G_L(j\omega) = G_{PD}(j\omega)S(j\omega), \quad (7)$$

and $G_{L,m}(j\omega)$ denotes the model of the linear dynamics $G_L(j\omega)$. By the robust-inversion technique, a frequency-dependent gain-modulation $\alpha(\omega)$ is introduced in the inversion-based ILC filter,

$$L(j\omega) = \alpha(\omega) \cdot G_{L,m}^{-1}(j\omega), \quad (8)$$

and then the design objective is transformed to finding the optimal gain modulation $\alpha(\omega)$ against the model uncertainty,

$$\min_{\alpha(\omega)} \sup_{\Delta G} |1 - \alpha(\omega)\Delta G(j\omega)| \quad (9)$$

The solution to the above minmax problem (9) is given in the following Theorem [7].

Theorem 1: At any given frequency ω , let the magnitude variation of the system dynamics $\Delta r(\omega)$ (defined in (6)) be bounded from below and from above by constants $\Delta r_{\min}(\omega) \in (0, 1]$ and $\Delta r_{\max}(\omega) \geq 1$, respectively, then

1) The optimal value of the minmax problem (9) is less than 1 if and only if

- a) the size of the phase variation of the system dynamics, $\Delta\theta_m(\omega)$, is less than $\pi/2$, i.e., $|\Delta\theta_m(\omega)| < \pi/2$; and
- b) the gain coefficient $\alpha(\omega)$ is chosen as

$$0 < \alpha(\omega) < \frac{2 \cos(\Delta\theta_m(\omega))}{\Delta r_{\max}(\omega)};$$

2) The optimal gain $\alpha(\omega)$, upon any bounded dynamics variation, is given by

$$\alpha_{opt}(\omega) = \frac{2 \cos(\Delta\theta_m(\omega))}{\Delta r_{\min}(\omega) + \Delta r_{\max}(\omega)}. \quad (10)$$

3) By using the optimal gain in (10), the solution to the minmax problem (9) is,

$$\begin{aligned} \min_{\alpha(\omega)} \sup_{\Delta G} |1 - \alpha(\omega)\Delta G(j\omega)| \\ = \frac{\cos(\Delta\theta_m(\omega)) \sqrt{2\Delta r_{\min}^2(\omega) + \Delta r_{\max}^2(\omega)}}{\Delta r_{\min}(\omega) + \Delta r_{\max}(\omega)} < 1 \end{aligned} \quad (11)$$

Corollary 1: The inversion-based ILC filter $L(j\omega)$ has no poles on the $j\omega$ axis, provided that the original system $G_{L,m}(j\omega)$ is hyperbolic (i.e., has no poles/zeros on the $j\omega$ axis).

Theorem 1 implies that when the phase variation is larger than or equal to $\pi/2$ at frequency ω , the optimal gain $\alpha(\omega)$ should be chosen to be zero, i.e., $L(j\omega) = 0$. When the model uncertainty is large, and the solution to the minmax problem (Eq. (5)) equals to one at that frequency ω . It is noted that the inversion-based filter $L(j\omega)$ might have poles on the open right half complex plan, thereby becomes unstable. Thus its online implementation, as needed in the proposed CCF-IIC algorithm, can be challenging. In the paper, the filter $L(j\omega)$ can be directly implemented in frequency-domain using Fourier-transform (FFT).

B. Design of the roll-off ILC filter $Q(j\omega)$

Next, the roll-off ILC filter $Q(j\omega)$ is designed to compensate for the system model uncertainties and noise effect. By Eq. (3), to guarantee the convergence of the CCF-ILC approach, the roll-off filter $Q(j\omega)$ must be chosen to render the iteration coefficient $\rho(j\omega)$ less than one (see Eq. (3)). Such a requirement leads to the following upper bound of the roll-off ILC filter $Q(j\omega)$:

$$|Q(j\omega)| < \frac{1}{|(1 - L(j\omega)G_{PD}(j\omega)S(j\omega))|} \quad (12)$$

To reduce the ultimate error $|e_\infty|$ (see Eq. (2)), the roll-off filter $Q(j\omega)$ should be close to one whenever it is possible. Since in practices, precision tracking at low frequency is usually needed, the roll-off filter $Q(j\omega) = 1$ should be

chosen in the low frequency range. In the high frequency range, however, model uncertainty tends to be significant with the phase variation larger than $\pi/2$, for example, around the resonant frequencies and/or lightly-damped zeros. Moreover, the noise and the disturbance effects also tend to be large—compared to the gain of the system—in the high frequency range. Therefore, the filter $Q(j\omega)$ should be rolled-off as frequency increases. Hence, the roll-off filter $Q(j\omega)$ should have “low-pass” characteristics, and Eq. (12) provides the guild in designing such a low-pass filter.

The phase delay, associated with conventional low-pass filters, however, must be carefully addressed when implementing the roll-off filter $Q(j\omega)$. To remove such a detrimental phase delay, a zero-phase low-pass filter is proposed to implement the roll-off filter $Q(j\omega)$. Particularly, a discrete-time domain representation of the zero-phase low-pass filter is presented here to facilitate its implementation [11]. The $2N$ order zero-phase FIR (finite impulse response) real filter has the form

$$Q(z) = b_0 + \sum_{k=1}^N (b_k z^k) + \sum_{k=1}^N (b_k z^{-k}) \quad (13)$$

where the coefficients $b_k \in \mathfrak{R}$. It can be shown that the frequency response of $Q(e^{j\omega T})$ is real. Thus, the phase of $Q(z)$ is zero. It is evident from Eq. (13) that the zero-phase FIR filter is noncausal. Such a noncausal filter, however, is implementable in the proposed CCF-ILC framework, because the signal to be filtered is the sample profile from the previous scanline, thereby completed known ahead.

C. Design of the sample topography observer $R(j\omega)$

Finally, we present a model-based sample topography observer $R(j\omega)$. In commercial AFMs, sample profile is estimated simply by scaling the input voltage to the z -axis piezo actuator with the DC-Gain of the piezo actuator. Large imaging distortion can be generated with such a method at high-speed scanning, because 1) the dynamics induced probe vibration and 2) the x -to- z dynamics coupling become significant at high-speed scanning. Therefore, new sample estimation method must be developed for high-speed AFM imaging. We estimate the sample profile by using the z -axis dynamics model. Note that the x -to- z dynamics-coupling can be regarded as an extra disturbance that effects the cantilever deflection, thus it can be accounted-for by replacing the sample topography $d(j\omega)$ in Fig. 1 (c) with

$$\hat{d}(j\omega) = d(j\omega) + d_c(j\omega) \quad (14)$$

where $d_c(j\omega)$ denotes the coupling caused disturbance input. Therefore, from the block diagram in Fig. 1 (c), the unknown sample topography (disturbance) signal $\hat{d}(\omega)$ can be represented as

$$\begin{aligned} \hat{d}(j\omega) &= -S^{-1}(j\omega)e_k(j\omega) - G_{PD}^{-1}(j\omega)u_{k,FF}(j\omega) \\ &\triangleq R(j\omega) \begin{bmatrix} e_k(j\omega) \\ u_{k,FF}(j\omega) \end{bmatrix}. \end{aligned} \quad (15)$$

Combining the above two Eqs. (14, 15), the sample topography $d(j\omega)$ can be estimated as

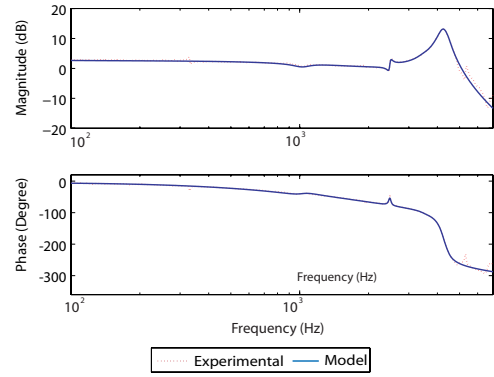


Fig. 2. The comparison of experimentally-measured nominal frequency response with the frequency response of the transfer function model for the AFM z -axis direction.

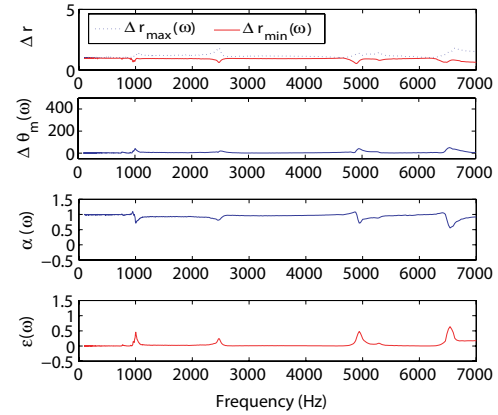


Fig. 3. The experimentally measured magnitude variation $\Delta r_{max}(\omega)$ and $\Delta r_{min}(\omega)$ (a), and phase variation $\Delta\theta_m(\omega)$ (b), and the calculated optimal gain $\alpha_{opt}(\omega)$ and the minimized solution $\epsilon_L(\omega)$ (d).

$$d(j\omega) = R(j\omega) \begin{bmatrix} e_k(j\omega) \\ u_{k,FF}(j\omega) \end{bmatrix} - d_c(j\omega). \quad (16)$$

Note that the cantilever deflection error, $e_k(j\omega)$, is utilized in the above sample topography estimation method, which implies that a good sample estimation can be obtained even when the z -axis positioning errors is relatively large (we note that precision positioning in the z -axis, however, is still needed in many AFM imaging applications).

IV. EXPERIMENT EXAMPLE: AFM IMAGING

We illustrate the proposed CCF-ILC approach by implementing it on an AFM system (*DimensionTM 3100*, Veeco Inc). We start with describing the controller design.

A. Controller Design

First, the frequency response of the AFM vertical (z -axis) dynamics, $G_{PD}(j\omega)$, was measured by using a data acquisition system along with MATLAB toolboxes as discussed in Ref. [7]. Then robust feedback controller was designed to satisfy the performance requirement as well as robustness requirement [7]. It is noted that a proportional-integral (PI) feedback controller was also designed for comparison. At last, the two ILC filters can be designed as follows.

Design of the inversion-based ILC filter $L(j\omega)$ We designed the inversion-based ILC filter $L(j\omega)$ by using

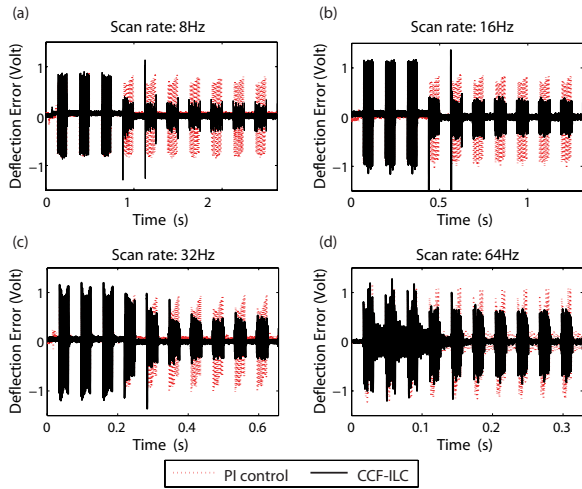


Fig. 4. Comparison of the deflection error (residual error) by using PI controller with that by using the proposed CCF-ILC approach for the four different scan rates of (a) 8Hz, (b) 16Hz, (c) 32Hz, and (d) 64Hz in one scanline imaging, where total of 10 repeated scan results are shown, and the feedforward control input was applied starting from the fourth scan;

the robust-inversion approach. As shown in Sec. III, the closed-loop frequency response $G_{L,m}(j\omega)$ and its dynamics uncertainty $\Delta G(j\omega)$ need to be obtained in order to design the filter $L(j\omega)$. Similar with the procedure discussed in Ref. [7], the closed-loop frequency response used in the ILC inversion-based filter design, $G_{L,m}(j\omega)$, was obtained by averaging closed-loop frequency responses $G_L(j\omega)$; the upper bound of the amplitude uncertainty and the phase uncertainty were estimated by finding the maximum difference among the experimental frequency responses; and finally the optimal gain coefficient $\alpha_{opt}(\omega)$, as well as the ILC filter $L(j\omega)$, can be designed according to Theorem 1. The results are shown in Fig. 3. In the experiments, the filter $L(j\omega)$ was implemented in frequency-domain using FFT/IFFT algorithm online. Hence no transfer function model and/or state-space time-domain model were needed.

Design of the roll-off ILC filter $Q(j\omega)$ The design of the ILC roll-off filter $Q(j\omega)$ as a zero-phase, low-pass filter is realized by combining a linear phase FIR low-pass filter with linear phase lead, $Q(z) = Q_l(z) \times z^P$ where $Q_l(z)$ is the linear-phase FIR low-pass filter (Matlab command “firpm”). Note that the phase lead term z^P is nothing but a forward shift of P -step in discrete-time implementation. Also the signal $L(j\omega)e_k(j\omega)$ and the feedforward control signal $u_{k,FF}(j\omega)$ from the previous scanline was delayed by one period of scan and then used as the input in the CCF-ILC algorithm, i.e., residual error signal was delayed by N -step (N : number of sampling points per scanline) in implementations.

B. Experimental results and discussion

The experimental implementation was conducted in two stages. First, the proposed method was used to repeatedly image a calibration sample on one scanline. Then secondly to show the efficiency of sample estimation, “One point imaging” was conducted, where a trajectory that mimicked a calibration sample profile on one scanline was injected as a disturbance to the z-axis piezo actuator.

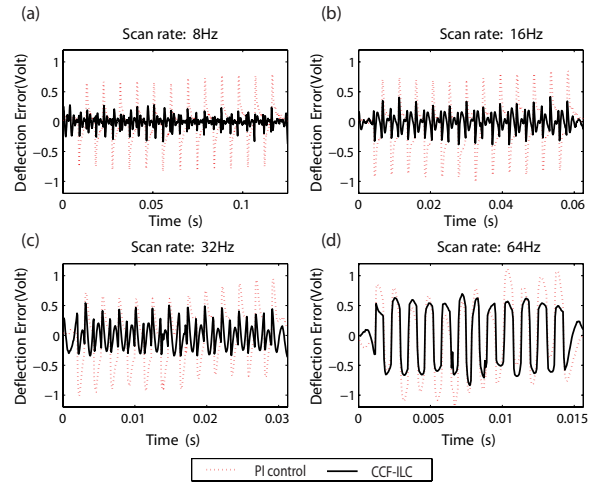


Fig. 5. Comparison of the deflection error (residual error) of PI controller and CCF-ILC approach for the four scan rates of (a) 8Hz, (b) 16 Hz, (c) 32 Hz, and (d) 64Hz in one scanline imaging, where one period results are shown.

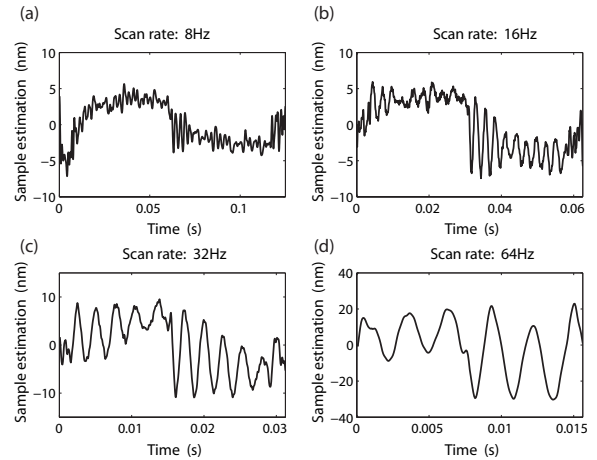


Fig. 6. Dynamics-coupling caused disturbance $d_c(t)$ for four scan frequencies (a) 8 Hz, (b) 16 Hz, (c) 32 Hz, and (d) 64Hz

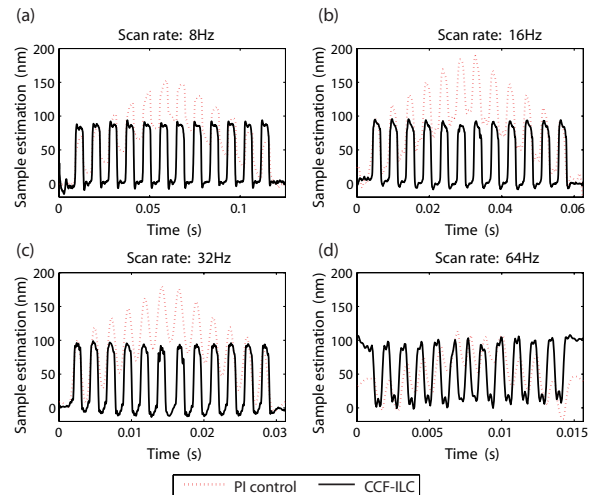


Fig. 7. Comparison of the estimated sample profile of PI controller and CCF-ILC approach for the two scan frequencies (a) 8Hz, (b) 16 Hz, (c) 32 Hz, and (d) 64Hz in one scan line imaging.

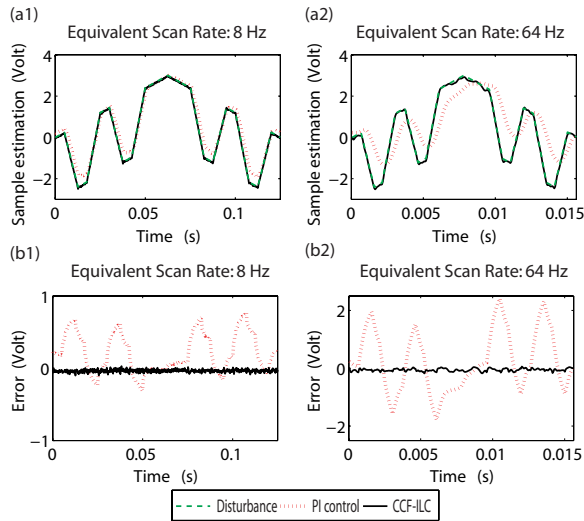


Fig. 8. Comparison of (a) the estimated 'sample profile', and (b) the estimation error of PI controller and CCF-ILC approach for two equivalent scan rates of (1) 8 Hz (2) 64 Hz in one point imaging.

One scanline imaging The proposed CCF-ILC technique was implemented to repetitively scan a calibration sample (TGZ02, MikroMasch, with a nominal pitch size of $3 \mu\text{m}$ and nominal step height of 84 nm) on the same scanline. The precision positioning in the lateral scanning was achieved by the inversion-based iterative control (IIC) approach [2], with the maximum relative tracking error $< 1\%$ of the scan range ($20 \mu\text{m}$) for four different scanning rates in the experiments, 8 Hz , 16 Hz , 32 Hz , and 64 Hz . The obtained deflection error signals are compared with those obtained by using the PI control, as shown in Fig. 4 (for the total of 10 periods scanning) and Fig. 5 (for the one period). The experimental results show that by using the proposed CCF-ILC approach, much smaller residual error was obtained than that by using the feedback control only. As shown in Fig. 4 (a), for the scan rate of 8 Hz , the maximum residual error under the CCF-ILC approach was 3 times smaller than that under the robust feedback control or under the PI control (The deflection error for the first three periods scanning under the CCF-ILC was obtained by using the robust feedback control only). Such small residual error was almost maintained when the scan rate was doubled and quadrupled (see Fig. 4 (b) and (c)). Even at the scan rate of 64 Hz , the residual error by using the CCF-ILC approach was still maintained as small as that by using the feedback control only at 8 times lower scan rate (compare Fig. 4 (a) with (d)). The proposed CCF-ILC approach was also used to quantify the dynamics-coupling caused disturbance ($d_c(j\omega)$ in Eq. 16), by scanning a flat sample surface at the four different scan rates (as shown in Fig. 6). Then the obtained dynamics-coupling disturbances were removed in the estimated sample profile by using the proposed sample estimator $R(j\omega)$ (see Sec. III-C). As shown in Fig. 7, good sample estimation was obtained by using the proposed estimator even at high-speed (32 Hz and 64 Hz), whereas the commercial DC-Gain estimation resulted in large sample distortions.

One point imaging The simulation-generated sample pro-

file mimics a calibration sample on one scanline with sample slope (which generally exists in real samples), and two different scanning rates were used in the experiments, 8 Hz and 64 Hz . Then the CCF-ILC approach was used to account for such a disturbance trajectory and the 'sample profile' can be estimated by using the observer $R(j\omega)$ as discussed in Sec. III-C. For comparison, a PI controller was also implemented, and the control signals were used to estimate the sample profile as in commercial AFM. The experiment results (as shown in Fig. 8) demonstrate that the proposed CCF-ILC approach can significantly lower the sample estimation error during high-speed scanning than what PI feedback control only can do.

V. CONCLUSION

A current cycle feedback iterative learning control approach was proposed in this article for the z -axis precision positioning. First, The convergence of this CCF-ILC approach was investigated. Then the controller design procedure was proposed: 1) design robust feedback controller using H_∞ method; 2) design inversion-based ILC filter using robust-inversion-based feedforward method; and 3) design the complementary roll-off ILC filter based on the already designed feedback controller and the inversion-based ILC filter. Finally, the implementation of the CCF-ILC algorithm on an AFM system were presented to show that smaller tracking error and better sample estimation can be achieved by using CCF-ILC algorithm than feedback only situation.

REFERENCES

- [1] K.-B. Lee, S.-J. Park, C. A. Mirkin, J. C. Smith, and M. Mrksich, "Protein nanoarrays generated by dip-pen nanolithography," *Science*, vol. 295, no. 5560, pp. 1702–1705, 2002.
- [2] Y. Wu and Q. Zou, "Iterative control approach to compensate for both the hysteresis and the dynamics effects of piezo actuators," *IEEE Trans. on Control Systems Technology*, vol. 15, no. 5, pp. 936–944, 2007.
- [3] O. M. El Rifai and K. Youcef-Toumi, "Trade-offs and performance limitations in mechatronic systems: A case study," *Annual Reviews in Control*, vol. 28, no. 2, pp. 181–192, 2004.
- [4] S. Hu and A. Raman, "Chaos in atomic force microscopy," *Physical Review Letters*, vol. 96, no. 3, p. 0361072, 2006.
- [5] G. Schitter, A. Stemmer, and F. Allgower, "Robust 2DOF-control of a piezoelectric tube scanner for high-speed atomic force microscopy," in *Proceedings of American Control Conference*, (Denver, CO), pp. 3720–3725, June 2003.
- [6] S. Skogestad and I. Postlethwaite., *Multivariable Feedback control: Analysis and Design*. New York: Wiley, second ed., 2005.
- [7] Y. Wu and Q. Zou, "Robust-inversion-based 2DOF-control design for output tracking: Piezoelectric actuator example," (New Orleans), pp. 2451 – 2457, IEEE, December 2007.
- [8] M. S. Salapaka, T. De, and S. Abu, "A robust control based solution to the sample-profile estimation problem in fast atomic force microscopy," *International Journal of Robust and Nonlinear Control*, vol. 15, pp. 821–837, 2005.
- [9] M. Verwoerd, G. Meinsma, and T. de Vries, "On admissible pairs and equivalent feedback – youla parameterization in iterative learning control," *Automatica*, vol. 42, pp. 2079–2089, 2006.
- [10] S. Tien, Q. Zou, and S. Devasia, "Iterative control of dynamics-coupling-caused errors in piezoscanners during high-speed AFM operation," *IEEE Trans. on Control Systems Technology*, vol. 13, no. 6, pp. 921–931, 2005.
- [11] J. Li and T.-C. Tsao, "Robust performance repetitive control systems," *Journal of Dynamic Systems, Measurement, and Control*, vol. 123, pp. 330–337, September 2001.